Hindawi
Journal of Sensors
Volume 2019, Article ID 8574750, 12 pages
https://doi.org/10.1155/2019/8574750

Research Article

Concrete Spalling Detection for Metro Tunnel from Point Cloud Based on Roughness Descriptor

Hangbin Wu, Xingran Ao, Zhuo Chen, Chun Liu, Zeran Xu, and Pengfei Yu

College of Surveying and Geo-Informatics, Tongji University, Shanghai 200092, China

Correspondence should be addressed to Zhuo Chen; czhuo0916@tongji.edu.cn

Received 20 January 2019; Revised 4 April 2019; Accepted 14 April 2019; Published 2 May 2019

Guest Editor: Sang-Hoon Hong

Automatic concrete spalling detection has become an important issue for metro tunnel examinations and maintenance. This paper focuses on concrete spalling detection research with surface roughness analysis based on point clouds produced by 3D mobile laser scanning (MLS) system. In the proposed method, at first, the points on ancillary facilities attached to tunnel surface are considered as outliers and removed via circular scan-line fitting and large residual error filtering. Then, a roughness descriptor for the metro tunnel surface is designed based on the triangulated grid derived from point clouds. The roughness descriptor is generally defined as the ratio of surface area to the projected area for a unit, which works well in identifying high rough areas on the tunnel surface, such as bolt holes, segment seams, and spalling patches. Finally, rough area classification based on Hough transformation and similarity analysis is performed on the identified areas to accurately label patches belonging to segment seams and bolt holes. After removing the patches of bolt holes and segment seams, the remaining patches are considered as belonging to concrete spalling. The experiment was conducted on a real tunnel interval in Shanghai. The result of concrete spalling detection revealed the validity and feasibility of the proposed method.

1. Introduction

Different from on-ground infrastructure, tunnels are always under the complex environmental conditions and constant heavy traffic loads. It is not uncommon to have damage on the tunnel surface due to the possibility of external forces and material deterioration [1, 2]. Therefore, during the service period of a tunnel, regular inspection activities should be carried out to check its health condition and regular maintenance measures should be taken to keep its structural integrity and ensure the safety in the operation process [3].

A concrete spalling [4–6], as shown in Figure 1, is a small but nonneglected tunnel damage which refers to the happening of surface defects whose depths are deeper than normal scaling, caused by material deformation or fragile deterioration. Concrete spalling is one of the most serious problems that affects the performance and reliability of a tunnel [7]. Traditionally, concrete spalling can be detected by human visual inspection, which needs tools of measuring tapes or profilers and to be identified by the size and location [8]. However, the process of manual inspection is time consuming and with low efficiency, and its result is also subjective and not reliable [9–12]. Therefore, it is urgent to replace the traditional method with a more accurate and automatic sensor-based method.

Currently, there are many researches focusing on detecting surface damage of concrete infrastructure with data gathered by different types of sensors. These researches can be generally classified in two ways. The first and preferred way is the approach of visual imaging and analysing to detect concrete surface damage, whose main advantages are the contactless technique, high speed in digital image acquisition, and the application of highly automated analysis procedures. For example, Dawood et al. [13] presented an integrated framework for the detection and quantification of concrete spalling distress from the digital images. The framework includes a hybrid algorithm for the detection of concrete spalling regions, interactive 3D presentation, and regression analysis to estimate the relationship between spalling intensity and depth. Medina et al. [14] applied a new method called Gabor filter invariant to rotation, allowing the detection of cracks in any direction from the tunnel images.

Figure 1: Concrete spalling image.

German et al. [15] retrieved the spalling properties from concrete column images in an attempt to assess the safety of postearthquake concrete structures. Koch and Brilakis [16] used histogram-based thresholds to segment the image into defective and nondefective regions and then approximated the defective shapes using morphological refinement and elliptic regression. Hutchinson et al. [17] presented a statistical method based on Bayesian decision theory for the purpose of detecting concrete damage (cracks, spalling, etc.) through conducting edge analysis of images. However, the requirement of illumination is essential for the camera to obtain high quality visual images, which usually cannot be satisfied since there is no enough light in a tunnel and it is hard to find a long-time lasting power for the long range tunnel inspection.

The second class of laser scanning approach, as an active detection technique, which can obtain high quality 3D point cloud data even in the weak illumination, has become more and more popular in the civil engineering domain in recent years [18–20]. For example, Teza et al. [21] used datasets collected by the terrestrial laser scanner to identify concrete surface damage using the mean curvature and Gaussian curvature of the structure surface, the application of which makes it possible to locate and quantify surface damage, so as to enhance the current visual inspection strategy. Mizoguchi et al. [22] evaluated the depth of scaling defects based on a customized region growing approach and iterative closest point (ICP) algorithm. Liu et al. [23] proposed a surface damage detection algorithm, known as light detection and ranging-based bridge evaluation (LiBE) for quantifying material quality loss. The LiBE algorithm distinguishes information obtained from the original concrete surface by calculating the surface gradient and displacement. Tang et al. [24] showed how laser scanners can be effectively used to assess surface flatness and that it is possible to detect surface flatness defects as small as 3 cm across and 1 mm thick from a distance of 20 m. Yoon et al. [25] proposed a method to detect cracks from laser scanned tunnel data using radiometric and geometric properties of laser points. Nevertheless, how to detect concrete spalling on the tunnel surface has not been fully discussed. This is because the effective models for spalling detection mostly focused on the planar concrete surface, while the nonplanar tunnel surface is still not established, which causes the concrete spalling in tunnels to not be accurately detected.

In this paper, we propose a novel method that can automatically detect the concrete spalling damage on tunnel surface from 3D point cloud obtained by mobile laser scanning system. The captured point cloud data not only contains information of the tunnel inner wall, but also includes outlier points such as ancillary facilities and subway tracks. Thus, firstly, the outlier points need to be removed via circular scan-line fitting and large residual error filtering. Then, a roughness descriptor for the metro tunnel surface is designed based on the triangulated grid derived from point clouds. The roughness descriptor is generally defined as the ratio of surface area to the projected area for a unit, which works well in identifying high rough areas on the tunnel surface, such as bolt holes, segment seams, and spalling patches. Finally, rough area classification based on Hough transformation and similarity analysis is performed on the identified areas to accurately label patches belonging to segment seams and bolt holes. After removing the patches of bolt holes and seams, the remaining patches are considered as belonging to concrete spalling. Compared with previous studies, the proposed method has the following characteristics: (1) automatic concrete spalling detection for tunnel surfaces and (2) guidelines for choosing optimal scanning parameters.

2. Research Methodology

2.1. Overview of the Proposed Method. The proposed concrete spalling detection method for metro tunnel based on roughness descriptor can be generally divided into three steps, namely, outlier points removal, roughness descriptor construction, and rough area classification, as shown in Figure 2. Point clouds used for concrete spalling detection were collected by a mobile three-dimensional laser scanning system. The collected point cloud data not only contains the necessary information of tunnel surface, but also captures the unnecessary points such as cables, pipelines, and subway tracks. Therefore, firstly, these unnecessary outlier points, including some derived from ancillary facilities and the other from noise generated by the scanner, will be removed on account of residual error filtering via a deviation threshold. This part is introduced in Section 2.2.

Secondly, a roughness descriptor, which is defined by the ratio between surface area and projected area for a unit, is constructed and applied into the remaining points to evaluate the rough situation of the tunnel surface. To this end, based on the Poisson surface reconstruction method, both the remaining points on tunnel surface and its corresponding projected points on cylindrical surface are used to generate the irregular triangulation, and, furthermore, to calculate the surface area and projected area, respectively, whose calculation method is to find the sum of areas of first-order neighbourhood triangles around each point. Thus, the roughness descriptor can be constructed and then the high rough areas including bolt holes, segment seams, and concrete spalling on the tunnel surface can be identified. This part is given in Section 2.3.

Finally, a rough area classification algorithm is performed to separate bolt holes and segment seams from the rough

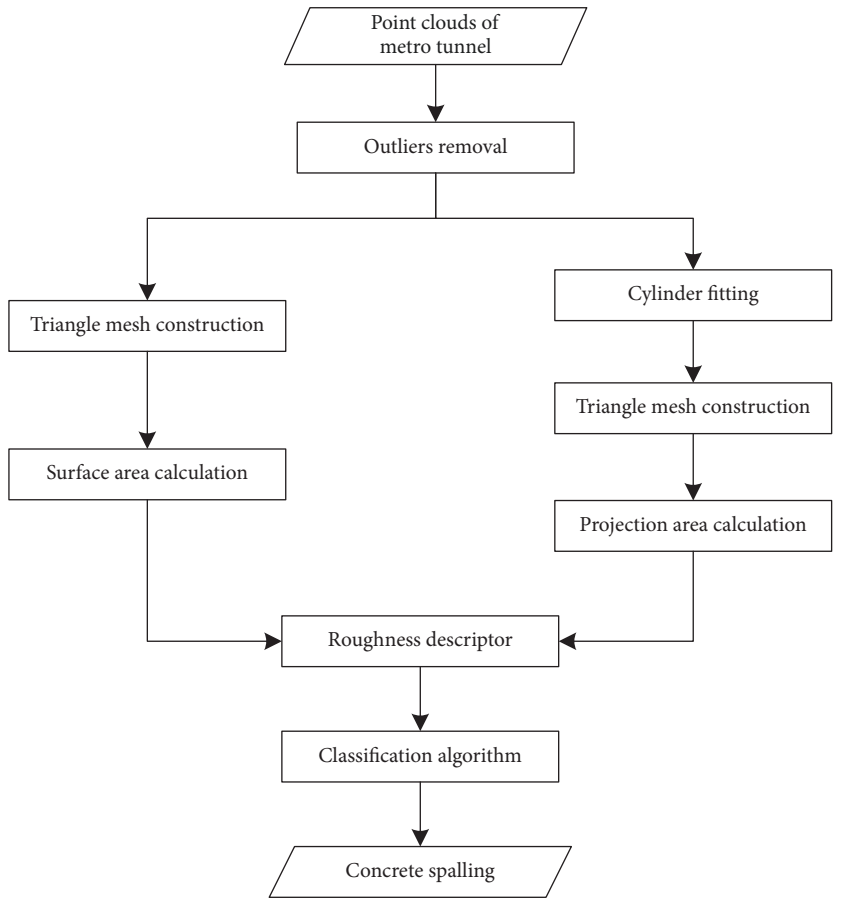

Figure 2: Flowchart of the proposed method.

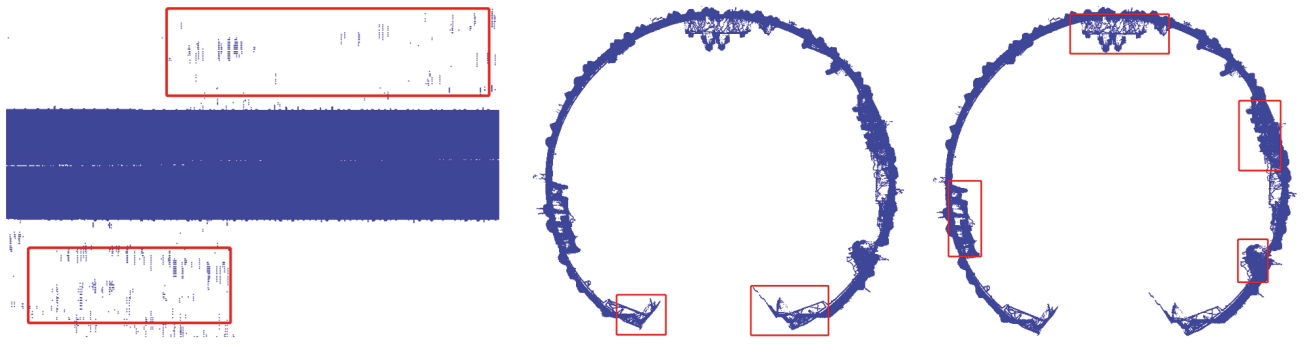

Figure 3: Three types of outlier points. (a) Drift points. (b) Redundant points. (c) Mixed points.

areas; thus the remaining patches are considered as belonging to concrete spalling. This is given in Section 2.4.

2.2. Outlier Points Removal. The point cloud used for concrete spalling detection is collected by a mobile three-dimensional laser scanning system that scans the tunnel surface in the form of a section during movement. Therefore, the captured point cloud data is stored as multiple scan lines, which not only contains the information of tunnel surface, but also captures the outlier points mainly originating from cables, lighting equipment, pipelines, and other facilities attached to the inner wall, subway tracks, and noise generated by the scanner. These outliers, however, inevitably affect the identification of concrete spalling and thus should be removed at the very beginning. In our method, the outlier points are roughly grouped into three categories according to spatial distribution, namely, drift points, redundant points, and mixed points, as shown in Figure 3.

The drift points are caused by the random noise generated by the laser scanner, whose spatial distribution is characterized as being dispersed and far away from the main part of metro tunnel. Thus, the drift points can be eliminated by the clustering algorithm. In addition, the redundant points come from subway track and other ground parts in metro tunnel, and the mixed points stem from some ancillary facilities. However, the two types of points are usually mixed with nonoutlier points of the tunnel surface; thus it is necessary to adopt an effective method to realize filtering.

Since the tunnel cross-section is designed as a standard circle, the captured point clouds present in the form of a large number of circular scanning lines. According to this, we propose a filtering algorithm to remove redundant points and mixed points by identifying points with large residual error. Each circular scan line is first fitted with a circle model by the RANSAC (random sample consistency) [26], in which the circle's boundary and centre are obtained. After that, the residual error can be calculated as the distance between each point on the scan line and the circle's boundary. Finally, the threshold of residual error is set and the points with residual errors larger than the threshold can be seen as outliers and removed.

2.3. Roughness Descriptor Construction. From the perspective of topography, surface roughness refers to the unevenness of the ground, generally defined as the ratio of the surface area to the projected area for a unit. It is usually used to reflect the high and low undulations on the terrain, the phenomenon of which has a similar shape to the undulations on the tunnel surface. Therefore, in this paper, the concept of surface roughness is introduced into the metro tunnel for the rough areas recognition.

2.3.1. Surface Area and Projected Area Calculation. A roughness descriptor needs to be constructed to identify the rough areas on tunnel surface. According to the definition of surface roughness (the ratio of surface area to the projected area for a unit), in our method, the surface area of a unit is represented by a polygon area enclosed by the points of the first-order neighbourhood around each point. Similarly, points on the tunnel surface are projected onto the cylindrical surface, and the polygon area of the first-order neighbourhood around each corresponding projected point is taken as the projected area of a unit.

Since the tunnel surface is nonplanar, in order to calculate the surface area or the projected area around each point, it is necessary to construct a triangular network for the point cloud of tunnel as well as the corresponding projected point cloud of cylinder, respectively. To this end, Poisson surface reconstruction [27] is adopted in this subsection, which is an intuitive method for mesh construction with point cloud and its normal vector serving as input components while the output manifests as a three-dimensional grid. Figure 4 shows the modelling results of a part of tunnel point cloud and the details of triangular mesh. Given the rough situation on tunnel surface, we do not calculate the area of the polygon enclosed by the points of the first-order neighbourhood, but the sum of triangular areas of the first-order neighbourhood around each point as the surface area of a unit.

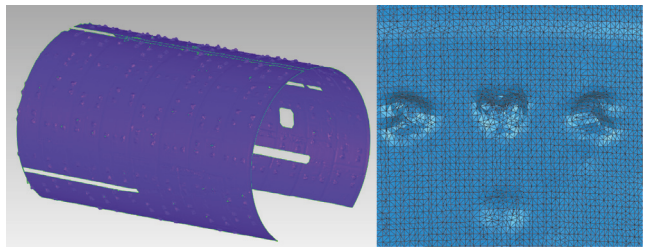

Figure 4: Triangular mesh of tunnel surface.

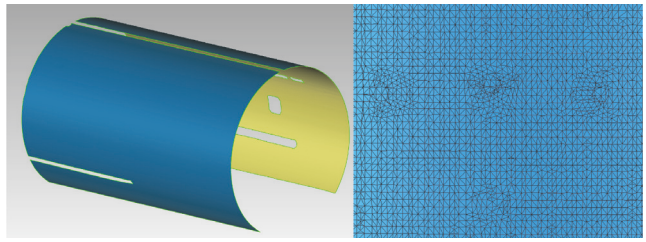

Figure 5: Triangular mesh of cylindrical surface.

What is more is that, for the sake of calculating the projected area, the corresponding relationship of points between tunnel and cylinder needs to be established accurately. Lei You et al. [28] proposed an algorithm for projecting trunk point clouds onto a cylindrical surface in sections to reconstruct the trunk surface, the theory of which is also applicable to the tunnel surface. Based on the algorithm, the tunnel surface can be defined by two parameters. The first one is centreline (L) that is described by a series of centre points $(c_i(c_x, c_y, c_z), i = 1, \cdots, n)$. The second parameter is the design diameter (d) of a metro tunnel. Taking into account the coordinate system of tunnel point cloud, Z axis is located at the vertical scanning plane with upward direction positive, and both X and Y axes are located at the lateral scanning plane and perpendicular to each other, which forms a right-handed coordinate system, wherein the positive direction of X axis points to the mileage direction. Thus, for any point $p(p_{x,}p_{y,}p_z)$ on the tunnel surface, its corresponding projection point p' on the cylindrical surface satisfies

$$\left\|\left(p' - \left(c_y, c_z, p_x\right)\right) \times (1, 0, 0)\right\| - d = 0 \tag{1}$$

where $\times$ is the outer product of vector, and $\|\ldots\|$ represents the modulus of the vector. It is noted that Equation (1) will have two solutions, taking the point close to p as the projection point p' on the cylindrical surface. Figure 5 shows the modelling results of a part of tunnel point cloud after projection and the details of triangular mesh. Then, according to the coordinates of projection points, the polygon area enclosed by the points of the first-order neighbourhood around each projection point is calculated as the projected area of a unit.

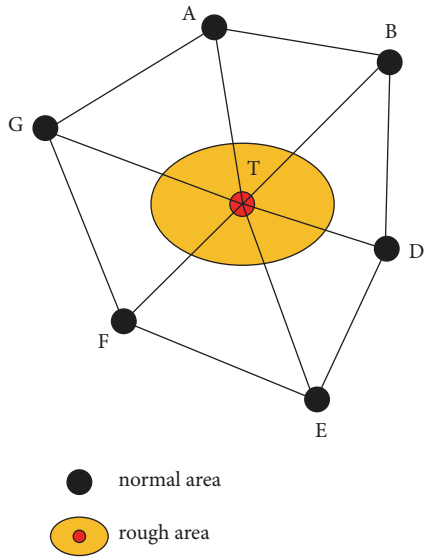

Figure 6: Sketch of rough area points.

2.3.2. Roughness Descriptor of Tunnel Surface. In this paper, we define the ratio of surface area to the projected area around each point as the roughness descriptor. After constructing the triangular mesh for the tunnel point cloud, it is necessary to calculate the area of each triangle and then find the sum of areas of first-order neighbourhood triangles around each point which is considered as the surface area of a unit. Similarly, point clouds on the cylindrical surface obtained from projection also need to generate a triangulated grid, where the polygon area enclosed by the points of the first-order neighbourhood for each point is performed as the projected area of a unit.

Simulating a set of points for a microelement on the tunnel surface, as shown in Figure 6, the black points represent normal area while the yellow zone represents the rough area. It is assumed that the red point T in the picture is in the rough area and other points, marked with A(x_1, y_1), B(x_2, y_2), and D(x_3, y_3), etc., are the normal points around T. The area of triangle which is made up of point T and the other two points around T can be calculated by Heron's formula [29] and stored. Taking the triangle ΔTAB as an example, lengths of the corresponding three sides are represented as t, a, and b, respectively, thus the area of which can be calculated by

$$S_{\Delta TAB} = \sqrt{q(q-t)(q-a)(q-b)} \quad q = \frac{(t+a+b)}{2}. \tag{2}$$

Therefore, the sum of triangle areas of the first-order neighbourhood around point T can be expressed as follows:

$$S_{tunnel} = \sum S_{\Delta} \tag{3}$$

Then, using the projection method described in Section 2.3.1 to generate projected points on cylindrical surface, the polygon area of the first-order neighbourhood around point T can be calculated by

$$\begin{aligned} S_{cylinder} &= S_{polygon(ABDEFG)} \\ &= \frac{1}{2}\sum_{i=1}^{n}(x_i + x_{i+1})(y_{i+1} - y_i) \end{aligned} \tag{4}$$

where n is the number of points around T. Accordingly, on the basis of definition of the roughness descriptor, a formula can be deduced as follows:

$$roughness = \frac{S_{tunnel}}{S_{cylinder}} = \frac{\sum S_{\Delta}}{S_{polygon}} \tag{5}$$

Finally, the roughness threshold should be set accurately to extract the points in high rough areas on tunnel surface.

2.4. Rough Area Classification. The points in rough areas on the surface of metro tunnel can be extracted by the roughness descriptor successfully, which are composed of three main categories, namely, concrete spalling patches, bolt holes, and segment seams. However, the three types of points extracted based on the roughness descriptor are mixed together, so we need to separate the points belonging to the concrete spalling patches from the rough points. In our method, taking into account the irregularity of spalling patches, we cannot directly identify them from rough areas. According to this, the method of rough area classification is adopted to accurately label patches belonging to segment seams and bolt holes so that the remaining patches are considered as belonging to concrete spalling.

For the seams between segments, if the tunnel point cloud is unfolded, the seam appears as a straight line. Thus, in this paper, the method for seam recognition is to project the point cloud of metro tunnel onto a plane and rasterize it into an image. After that, the Hough transform [30] is applied to recognize the lines so that the seams of tunnel segments can be determined and furthermore eliminated from the point cloud.

For the bolt holes, there is a fixed size; we can establish a standard point cloud template of bolt holes. The point cloud is then clustered, and the degree of similarity between each small clustered group and the template is compared based on the similarity analysis method to determine which small cluster belongs to bolt hole. In order to obtain the clustered point cloud of bolt hole, the mean-shift clustering algorithm [31] is applied to the remaining point cloud after seam elimination including bolt holes and spalling patches, so that the point clouds can form many different small groups. Meanwhile, we established the point cloud library of bolt hole to be regarded as a template for recognition. The size of bolt hole we used to collect the point cloud library is about 20∗14∗18 (cm) and 17∗15∗18 (cm). Based on the similarity comparison between the template and the clustered small groups, bolt holes can be identified from the point clouds. The specific implementation method is as follows. Firstly, it is necessary to standardize the position of template points and each clustered small group by performing PCA transformation (Principal

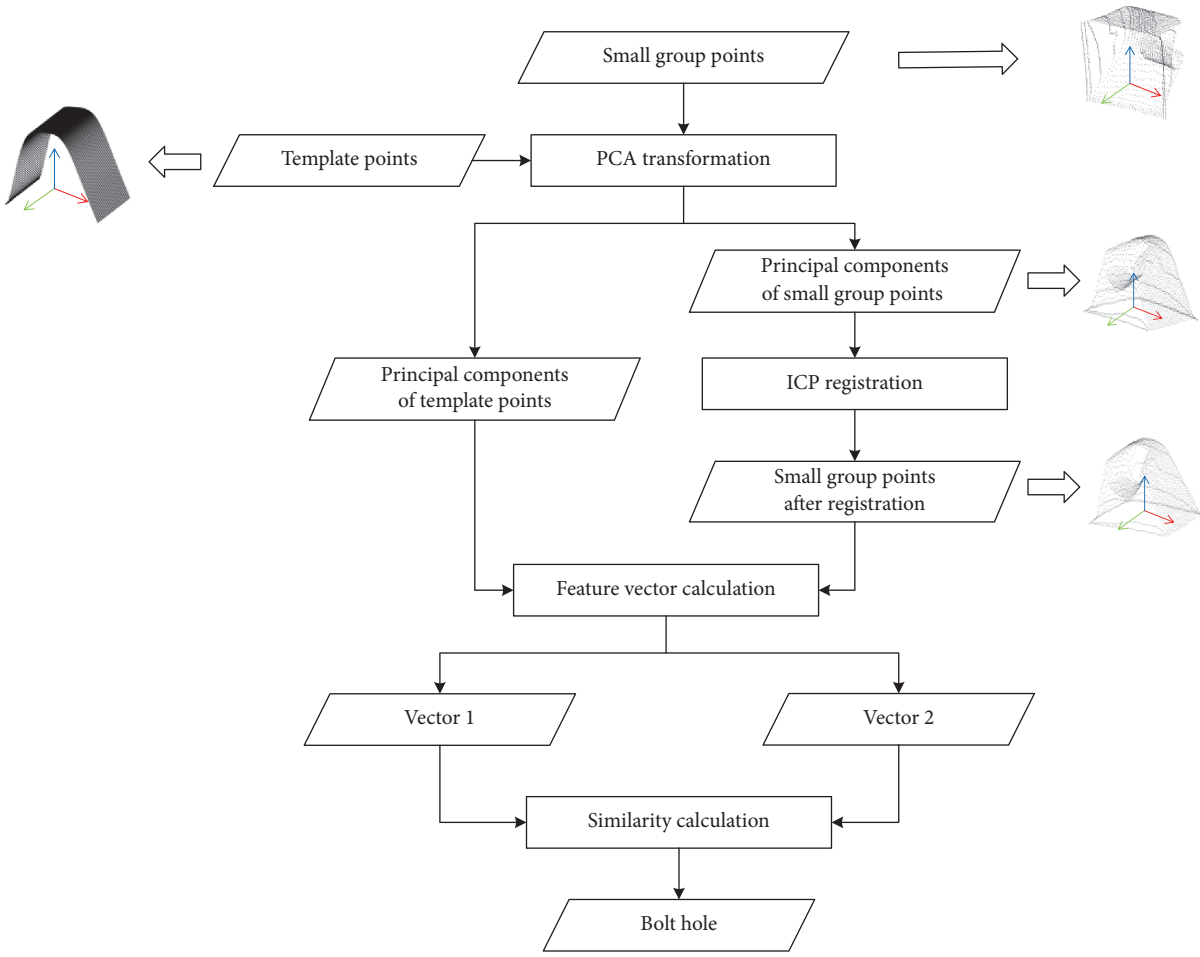

Figure 7: Procedure of bolt hole recognition.

Component Analysis) [32] on the two three-dimensional point clouds, so that the three main components of both are obtained and taken as the new standardized coordinate systems. Secondly, after the coordinate transformation, each small group is registered with the template by using the ICP (Iterative Closest Point) [33] registration algorithm to further adjust the clustered points so as to have a similar posture to the template as much as possible. Thirdly, calculate the feature vector of point cloud whose method is proposed by Xiaotong H et al. [34] for the principal components of the template and the registered small group points, respectively, and furthermore perform similarity comparison between the two feature vectors to distinguish bolt holes from rough points. Generally speaking, any small group of point clouds with similarity score greater than the accurate threshold can be identified as a bolt hole. The procedure of bolt hole recognition is shown in Figure 7.

2.5. Detectable Spalling Analysis. In this paper, we define the ratio of surface area to the projected area around each point as the roughness descriptor, and simultaneously a formula thereof has also been deduced in Section 2.3.2. What is more is that it is necessary to analyse the minimum spalling patches that can be extracted using this method in metro tunnel. Therefore, it is assumed that Figure 6 shows a microelement on the tunnel surface under the ideal conditions, where the point spacing is represented by m. The black point is in the normal area, whose depth is zero, while the red point is in the spalling area, and the depth is h. According to the roughness formula, the sum of areas of first-order neighbourhood triangles around point T can be expressed as

$$S_{tunnel} = \sum S_{\Delta} = 3m\sqrt{\left(\frac{3}{4}m^2 + h^2\right)} \tag{6}$$

And the polygon area of first-order neighbourhood around the projected point T can be expressed as

$$S_{cylinder} = S_{polygon} = \frac{3\sqrt{3}}{2}m^2 \tag{7}$$

Thus the roughness descriptor can be calculated as follows:

$$roughness = \frac{S_{tunnel}}{S_{cylinder}} = \frac{2\sqrt{3}}{3}\sqrt{\frac{3}{4} + \left(\frac{h}{m}\right)^2} \tag{8}$$

Hence one can see that, in the position where the spalling does not occur or the nonrough position, h=0; that is, the

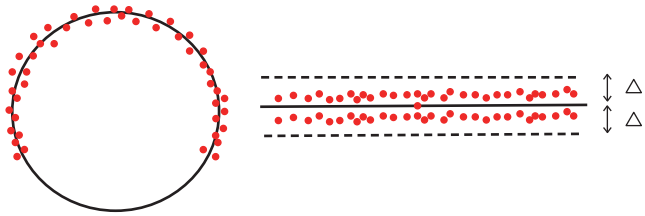

Figure 8: A scan line of tunnel point cloud. The black ring represents the real position of a section on the tunnel inner wall, and the deviation of red points away from black ring is regarded as the precision of point cloud (Δ).

value of roughness descriptor is 1. When h > 0, the value of roughness descriptor is greater than 1. It indicates that the position is rough relative to the normal position and may be spalling.

Therefore, the detectability of concrete spalling based on the roughness descriptor is determined by the spalling depth h and the point spacing m, while these two parameters are mainly affected by the instrument accuracy and the set parameters of the MLS system used when collecting point cloud in metro tunnel, namely, range error Δ and the resolution of laser scanner as well as the running velocity of MLS system. Firstly, the range error Δ of laser scanner indicates the precision of the collected point cloud of metro tunnel. Taking out a scan line of point cloud and expanding it into a straight line as shown by red points in Figure 8, assume that the black ring is the real position of a section on the tunnel inner wall while the deviation of captured points away from the inner wall is regarded as the precision of point cloud, which is represented by Δ. Thus it can be seen that the spalling patches will not be detected when the value of spalling depth h is less than Δ.

The other factor that affects the detectability of spalling is the point spacing m, including the vertical spacing and longitudinal spacing. The vertical spacing of point cloud depends on the resolution of the scanner. When setting different resolutions, the number of scanning points on the one scan-line changes accordingly. In addition, since the frequency of scanner is usually fixed, the velocity of the mobile laser scanning system determines the point spacing in the direction of the mileage, commonly referred to as the longitudinal spacing. Taking a microelement on the surface of tunnel as an example in Figure 9, the vertical and longitudinal spacing of point cloud are represented by m_1 and m_2, respectively, and the blue areas are used to indicate the spalling patches. It follows that, when the area of spalling patches less than the product of vertical spacing and longitudinal spacing, it cannot be detected either.

Therefore, when the depth h and the area S_c of a concrete spalling patch satisfy the following formula (9), it can be extracted from the point cloud of tunnel surface, which can also be used as a guideline to select optimal scanning parameters for MLS system:

$$\begin{aligned} h &> \Delta; \\ S_c &> m_1 * m_2. \end{aligned} \tag{9}$$

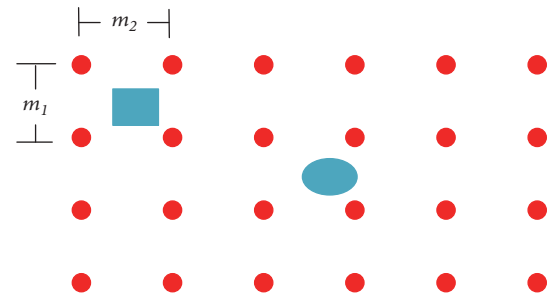

Figure 9: A microelement on tunnel surface. The red dots indicate the points on a microelement of tunnel surface captured by scanner, and the blue areas indicate the spalling patches.

Figure 10: Mobile laser scanning system.

3. Case Study

3.1. Data Collection of Metro Tunnel. A section of a metro tunnel in Shanghai was selected as the experimental area with a total length of about 250 meters. The mobile laser scanning (MLS) system is equipped with a scanner of FARO FOCUS3D X330 for point cloud data collection in the tunnel, as shown in Figure 10, the scanner of which has a scanning range of 300° and working frequency of 100 Hz. In order not to affect the routine operation of the subway, the experimental data acquisition was carried out between midnight and three in the morning. And the resolution of scanner is set to 1/4, so the number of points in one circular scan line is about 9760 and the vertical point spacing m_1 is about 2 mm. Generally, during the period of data acquisition, to ensure the density of point cloud, the running velocity of MLS system on the subway track is set to 0.5m/s, so the average point spacing m_2 of the collected point clouds in the mileage direction is about 5 mm. The general information of the case area and data collection is shown in Table 1.

3.2. Experimental Results

3.2.1. Outlier Removal Result of Tunnel Point Cloud. The captured point cloud data by MLS system mainly contains the information of the tunnel surface where it is also mixed with some outlier points originating from the subway tracks, cables, lighting equipment, and other facilities, which will inevitably have great interference on the concrete spalling

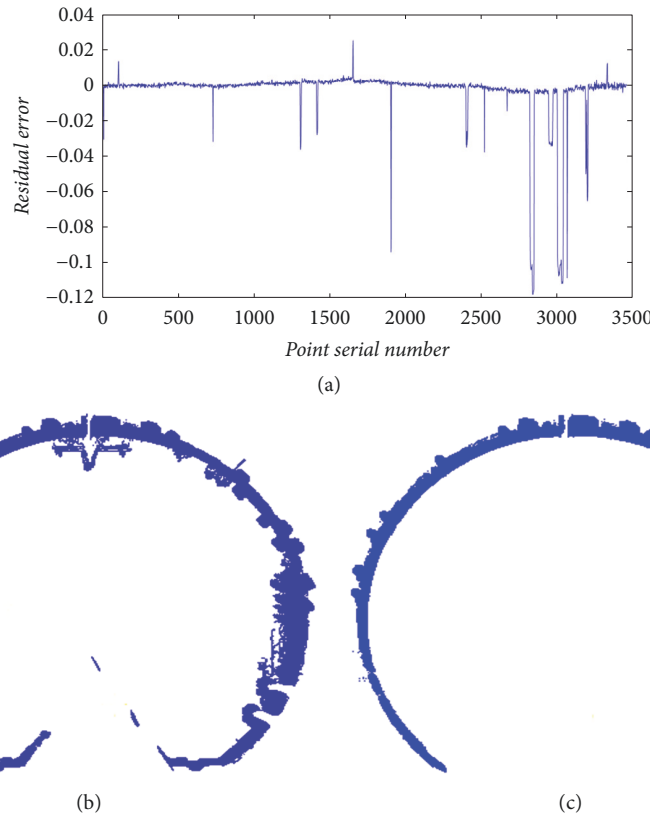

Figure 11: Outlier removal. (a) Residual error curve of one scan line, (b) before the outlier removal and (c) after the outlier removal.

Table 1: General information of the case area and data collection.

Parameters	Value
Length of case tunnel	250 m
Radius of the tunnel	2.75 m
Average velocity during data collection	0.5 m/s
Scanning distance	330 m
Scanning range	300°
Working frequency	100 Hz
Resolution	1/4
Range error (Δ)	2 mm
Vertical point spacing (m_1)	2 mm
Longitudinal point spacing (m_2)	5 mm
Point density	100,000 pts/m^2
Total points	> 500,000,000 pts

identification. Thus, according to the outlier points removal algorithm introduced in Section 2.2, the residual error curve for each circular scan line can be generated, an example of which is shown in Figure 11(a). Since the fluctuation range of residual errors is between plus and minus 0.01, hence it can be seen that points with an error of less than negative 0.01 can be considered outliers and then eliminated. Figures 11(b) and 11(c) show the point cloud of tunnel before and after outlier points removal, respectively.

Most of the outlier points with a certain distance from the tunnel surface can be removed using the residual error filtering algorithm. However, there are still a small fraction of points from the bottom of pipeline facility that clings to the tunnel inner wall and cannot be completely eliminated through this method, causing them to eventually be identified as rough areas. This part of points is usually presented in the form of a line, so it can be identified and further removed together with ring seams through the algorithm of Hough transformation later.

3.2.2. Rough Area Extraction. After removing the outlier points from original point cloud data of metro tunnel, a roughness descriptor based method is applied to extract the points of rough areas on tunnel surface for the purpose of further identifying the concrete spalling patches therefrom. Thus, in order to calculate the value of roughness descriptor for each point, triangular meshes are first constructed for both the remaining points after outlier removal and the corresponding projected points on the cylindrical surface, thereby obtaining the surface area and projected area of the first-order neighbourhood around each point. Then, according to the definition of roughness descriptor, the ratio of surface area to the projected area around each point is calculated, a histogram of which is also generated indicating the number of points corresponding to different roughness values, as shown in Figure 12.

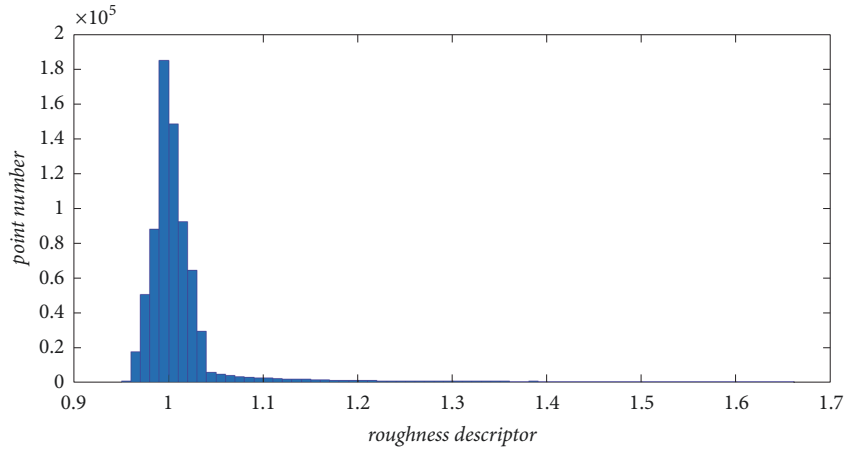

Figure 12: Histogram of roughness descriptor.

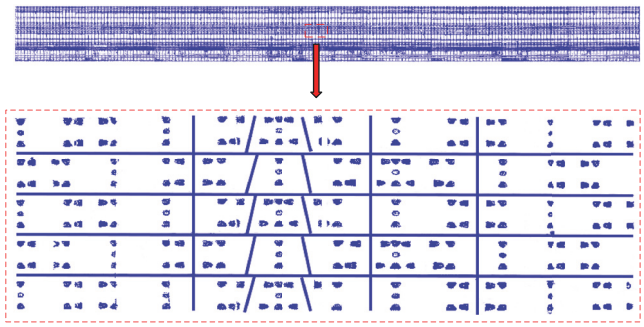

Figure 13: Roughness map of tunnel surface.

According to the value of the roughness descriptor for each point obtained, we need to determine an accurate threshold to extract the points belonging to rough areas. Taking into account the scanner accuracy and the set parameters of MLS system during operation, in this experiment mainly relying on the range error Δ and the point spacing m, the expression of roughness descriptor can be further represented as follows:

$$roughness = \frac{2\sqrt{3}}{3}\sqrt{\frac{3}{4} + \left(\frac{h+\Delta}{m}\right)^2} \tag{10}$$

It can be seen from formula (10) that when the value of the depth h for a certain point tends to zero, roughness ratio is at a critical condition. Therefore, with the value of point spacing m and range error Δ in this case study, the threshold of roughness descriptor has been obtained as about 1.05, and points with proportion greater than 1.05 are filtered as rough areas. Expand the rough point cloud on the tunnel surface into a plane as shown in Figure 13.

It should be noted that we cannot thin the original point cloud; otherwise some points belonging to rough areas may be missed, which will affect the detection of spalling damage. However, when calculating the roughness value of each point, the number of tunnel point clouds captured by MLS system is very huge, which will take a lot of time to find a polygon area surrounded by its first-order neighbourhood points for each point. Accordingly, BitMap and BloomFilter are adopted in this part to improve performing efficiency of the algorithm. Bitmap is a compact data storage structure that allocates 1 bit of memory for each element in the collection, which greatly reduces the storage space required to process massive point cloud data. Based on this structure, BloomFilter completes the query of the first-order neighbourhood points for each point, and then we can calculate the area of polygon enclosed by them, which greatly compresses the memory space and shortens the calculation time.

3.2.3. Results of Concrete Spalling Detection. The rough areas extracted on tunnel surface based on the method of roughness descriptor mainly contain three types of objects, namely, concrete spalling patches, bolt holes, and the seams between segments. In order to identify the points belonging to spalling patches, we used the method of rough area classification described in Section 2.4 to separate bolt holes and the segment seams from rough points, so that the concrete spalling patches can be remained.

Firstly, if the tunnel surface is unfolded into a plane, the seam appears as a line. Therefore, the method of seam identification is to project the rough point cloud extracted onto a plane and rasterize it into an image. Then the Hough transformation algorithm can be used to identify seams between segments, the result of which is shown in Figure 14. As we can see from the figure, seams including the transverse seams, longitudinal seams, and oblique seams have been identified successfully.

Then, the bolt holes are detected using the similarity analysis method, the separation result of which is shown in Figure 14, where the bolt holes are shown in blue blocks. The remaining patches belong to the concrete spalling area shown in red. After detecting the tunnel section of 250 m, it was found through statistics that the spalling patches mainly occurred in the subinterval between 175 and 200 m, so that, in order to express the detected spalling more clearly, Figure 14 shows the information of tunnel between 175 and 200 m. Finally, we found seven concrete spalling patches in this case

Table 2: Basic information of concrete spalling patches.

No.	Mileage [m]	Spalling patches	Images	Spalling area [m^2]	Spalling depth [m]
J1	176		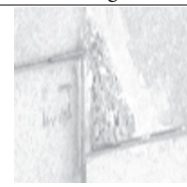	0.0191	0.112
J2	176			0.0276	0.126
J3	177		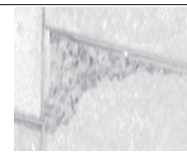	0.0377	0.195
J4	178			0.0340	0.099
J5	177		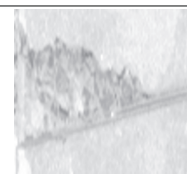	0.0384	0.129
J6	177		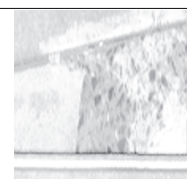	0.0681	0.083
J7	193			0.0249	0.091

study, the basic information of which is shown in Table 2, and the mileage position corresponding to the spalling is also given at the same time.

According to formula (9), the theoretical depth value and area value of minimum spalling patch are 2 mm and 10 mm^2, respectively, and the extracted results are indeed greater than the theoretical minimum.

In this paper, in order to examine the accuracy of the detected results, we conducted a joint manual inspection with the maintenance company on the seven detected spalling patches; that is, each of the spalling was confirmed one by one in the tunnel. It was found that each spalling did occur at the corresponding position. Therefore, the false detection rate is zero and it is confirmed that the proposed concrete spalling detection algorithm performs well. In addition, taking into account the small size of the spalling and the large spacing between the points, it does cause omission errors, which have been analysed in Section 2.5. However, these regions that

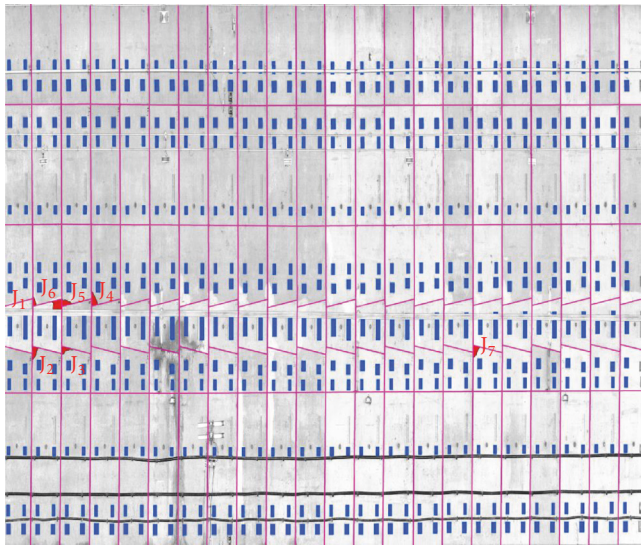

Segment seam
Bolt hole
Concrete spalling

FIGURE 14: Recognition result of bolt holes, segment seams, and concrete spalling patches in tunnel subinterval of 175-200 m.

could not be detected are very small and belong to the normal category, which will not affect the performance and reliability of a tunnel.

4. Conclusion

In this paper, a new method used for concrete spalling detection in metro tunnel from point cloud based on the roughness descriptor is proposed. Firstly, the point cloud acquired by mobile laser scanning system needs to eliminate outlier points originating from ancillary facilities attached to shield tunnel wall based on the residual error filtering algorithm. Then, a roughness descriptor for the metro tunnel surface is designed to extract the rough areas on the tunnel surface, including bolt holes, segment seams, and spalling patches. Finally, rough area classification is performed on the identified rough areas to accurately separate the segment seams and bolt holes from rough areas, so that the concrete spalling patches are left. A section of metro tunnel interval about 250 m in Shanghai is selected to verify the validity of the proposed method, and seven concrete spalling areas are detected which are identified as surface defects in metro tunnel. This could be helpful for tunnel maintenance and operation safety. Compared with previous studies, the concept of roughness descriptor is proposed to detect concrete spalling which is suitable for not only flat concrete surfaces but also nonplanar concrete surfaces, and, at the same time, offer the guidance for optimal scanning parameter selection.

Data Availability

The data used to support the findings of this study are available from the corresponding author upon request.

Conflicts of Interest

The authors declare that there are no conflicts of interest regarding the publication of this paper.

Acknowledgments

This research is supported by the National Science Foundation of China (no. 41671451), the National Science and Technology Major Program (2016YFB0502104), and the Fundamental Research Funds for the Central Universities of China. The authors would like to express appreciation to colleagues in our laboratory for their valuable comments help.

References

[1] T. Asakura and Y. Kojima, "Tunnel maintenance in Japan," *Tunnelling and Underground Space Technology*, vol. 18, no. 2-3, pp. 161–169, 2003.

[2] Y. Yuan, Y. Bai, and J. Liu, "Assessment service state of tunnel structure," *Tunnelling and Underground Space Technology*, vol. 27, no. 1, pp. 72–85, 2012.

[3] F. Sandrone and V. Labiouse, "Identification and analysis of Swiss National Road tunnels pathologies," *Tunnelling and Underground Space Technology*, vol. 26, no. 2, pp. 374–390, 2011.

[4] Portland Cement Association (PCA), *Concrete slab surface defects: Causes, Prevention, And Repair*, Portland Cement, Skokie, IL, USA, 2001.

[5] N. Delatte, S. Chen, N. Maini et al., "Application of nondestructive evaluation to subway tunnel systems," *Transportation Research Record*, vol. 1845, no. 3, pp. 127–135, 2003.

[6] H. Russell and J. Gilmore, "Inspection policy and procedures for rail transit tunnels and underground structures," *Transit Cooperative Research Program Synthesis of Transit Practice*, 1997.

[7] Y. Yuan, X. Jiang, and Q. Ai, "Probabilistic assessment for concrete spalling in tunnel structures," *ASCE-ASME Journal of Risk and Uncertainty in Engineering Systems, Part A: Civil Engineering*, vol. 3, no. 4, 2017.

[8] M.-K. Kim, H. Sohn, and C.-C. Chang, "Localization and quantification of concrete spalling defects using terrestrial laser scanning," *Journal of Computing in Civil Engineering*, vol. 29, no. 6, 2015.

[9] Z. Zhu and I. Bilakis, "Detecting air pockets for architectural concrete quality assessment using visual sensing," *Electronic Journal of Information Technology in Construction*, vol. 13, pp. 86–102, 2008.

[10] American Concrete Institute, *ACI Manual of Concrete Inspection*, ACI Committee 311, SP-2(07), Detroit, Mich, USA, 2007.

[11] A. M. Paterson, G. R. Dowling, and D. A. Chamberlain, "Building inspection: can computer vision help?" *Automation in Construction*, vol. 7, no. 1, pp. 13–20, 1997.

[12] B. Guldur Erkal and J. F. Hajjar, "Laser-based surface damage detection and quantification using predicted surface properties," *Automation in Construction*, vol. 83, pp. 285–302, 2017.

[13] T. Dawood, Z. Zhu, and T. Zayed, "Machine vision-based model for spalling detection and quantification in subway networks," *Automation in Construction*, vol. 81, pp. 149–160, 2017.

[14] R. Medina, J. Llamas, J. Gómez-García-Bermejo, E. Zalama, and M. Segarra, "Crack detection in concrete tunnels using a Gabor filter invariant to rotation," *Sensors*, vol. 17, no. 7, p. 1670, 2017.

[15] S. German, I. Brilakis, and R. Desroches, "Rapid entropy-based detection and properties measurement of concrete spalling with machine vision for post-earthquake safety assessments," *Advanced Engineering Informatics*, vol. 26, no. 4, pp. 846–858, 2012.

[16] C. Koch and I. Brilakis, "Pothole detection in asphalt pavement images," *Advanced Engineering Informatics*, vol. 25, no. 3, pp. 507–515, 2011.

[17] T. C. Hutchinson and Z. Chen, "Improved image analysis for evaluating concrete damage," *Journal of Computing in Civil Engineering*, vol. 20, no. 3, pp. 210–216, 2006.

[18] H. S. Park, H. M. Lee, H. Adeli, and I. Lee, "A new approach for health monitoring of structures: terrestrial laser scanning," *Computer-Aided Civil and Infrastructure Engineering*, vol. 22, no. 1, pp. 19–30, 2007.

[19] M. Hawarey and M. O. Falk, "Using laser scanning technology to measure deflections in steel columns," *Iron and Steel Technology*, vol. 1, no. 3, pp. 40–45, 2004.

[20] S. J. Gordon and D. D. Lichti, "Modeling terrestrial laser scanner data for precise structural deformation measurement," *Journal of Surveying Engineering*, vol. 133, no. 2, pp. 72–80, 2007.

[21] G. Teza, A. Galgaro, and F. Moro, "Contactless recognition of concrete surface damage from laser scanning and curvature computation," *NDT & E International*, vol. 42, no. 4, pp. 240–249, 2009.

[22] T. Mizoguchi, Y. Koda, I. Iwaki et al., "Quantitative scaling evaluation of concrete structures based on terrestrial laser scanning," *Automation in Construction*, vol. 35, pp. 263–274, 2013.

[23] W. Liu, S. Chen, and E. Hauser, "LiDAR-based bridge structure defect detection," *Experimental Techniques*, vol. 35, no. 6, pp. 27–34, 2011.

[24] P. Tang, D. Huber, and B. Akinci, "Characterization of laser scanners and algorithms for detecting flatness defects on concrete surfaces," *Journal of Computing in Civil Engineering*, vol. 25, no. 1, pp. 31–42, 2011.

[25] J. Yoon, M. Sagong, and J. S. Lee, "Development of damage detection method on the tunnel lining from the laser scanning data," in *Proceedings of the World Tunnel Congress 2007 and 33rd ITA/AITES Annual General Assembly*, pp. 1469–1474, 2007.

[26] A. Martin and C. Robert, "Random sample consensus: a paradigm for model fitting with applications to image analysis and automated cartography," *Communications of the ACM*, vol. 24, no. 6, pp. 381–395, 1981.

[27] M. Kazhdant, M. Bolitho, and H. Hoppe, "Poisson surface reconstruction," in *Proceeding SGP '06 Proceedings of the fourth Eurographics symposium on Geometry processing*, pp. 61–70, 2006.

[28] Y. Lei, Shouzheng T., and S. Xinyu, "An algorithm of stem surface reconstruction based on cylindrical projection," *Journal of Forest Research*, vol. 29, no. 6, pp. 812–819, 2016.

[29] W. Dunham, "Heron's formula for triangular area," in *Journey through Genius: The Great Theorems of Mathematics*, pp. 113–132, Wiley, New York, NY, USA, 1990.

[30] R. O. Duda and P. E. Hart, "Use of the Hough transformation to detect lines and curves in pictures," *Communications of the ACM*, vol. 15, no. 1, pp. 11–15, 1972.

[31] D. Comaniciu and P. Meer, "Mean shift: a robust approach toward feature space analysis," *IEEE Transactions on Pattern Analysis and Machine Intelligence*, vol. 24, no. 5, pp. 603–619, 2002.

[32] H. Hotelling, "Analysis of a complex of statistical variables into principal components," *Journal of Educational Psychology*, vol. 24, no. 7, pp. 498–520, 1933.

[33] P. J. Besl and N. D. McKay, "A method for registration of 3-D shapes," *IEEE Transactions on Pattern Analysis and Machine Intelligence*, vol. 14, no. 2, pp. 239–256, 1992.

[34] H. Xiaotong and W. Jiandong, "Similarity analysis of three-dimensional point cloud based on eigenvector of subspace," *Hongwai yu Jiguang Gongcheng/Infrared and Laser Engineering*, vol. 43, no. 4, pp. 1316–1321, 2014.